2.1.2. Artículo I

DE GRUYTER

OPTO-ELECTRONICS REVIEW **23**(1), 00–00

DOI: 10.1515/oere-2015-0006

Aerial thermography from low-cost UAV for the generation of thermographic digital terrain models

S. LAGÜELA*, L. DÍAZ-VILARIÑO, D. ROCA, and H. LORENZO

Applied Geotechnologies Research Group, University of Vigo, Lab 22, ETSE Minas, Campus Universitario Lagoas- Marcosende, 36310 Vigo, Pontevedra, Spain

Aerial thermography is performed from a low-cost aerial vehicle, copter type, for the acquisition of data of medium-size areas, such as neighbourhoods, districts or small villages. Thermographic images are registered in a mosaic subsequently used for the generation of a thermographic digital terrain model (DTM). The thermographic DTM can be used with several purposes, from classification of land uses according to their thermal response to the evaluation of the building print as a function of their energy performance, land and water management. In the particular case of buildings, apart from their individual evaluation and roof inspection, the availability of thermographic information on a DTM allows for the spatial contextualization of the buildings themselves and the general study of the surrounding area for the detection of global effects such as heat islands.

Keywords: aerial platform, infrared thermography, thermographic DTM, land uses, terrain classification.

1. Introduction

Infrared thermography has been widely used in buildings for the detection of construction defects such as air infiltrations, thermal bridges, and moisture areas [1–3], as well as the calculation of thermophysical parameters of the building materials [4–5] and the energy performance of the building as a whole [6–7]. In recent studies this information has been registered with a point cloud for its combination with geometric information towards its location and accurate measurement of the affected areas [8–9]. These studies are usually performed from a terrestrial point of view, either by an operator walking around the building [10], or by a terrestrial mobile platform from where data is acquired as a sequence [11]. Nevertheless, the principal drawbacks of these studies are that buildings are considered in isolation, not paying attention to their environment, and that the documentation process does not usually include details from difficult access areas such as roofs, where measurements are not possible in the common mode.

Up to date thermal satellite images and thermographic aircraft acquisitions are the most used technologies for providing temperature data of large areas from a bird's eye viewpoint. In both cases the resolution is usually not enough for capturing depict details of buildings due to the width of the areas covered unless panchromatic bands are used [12], and the applications usually focus on studying the behaviour of large areas as a whole, for example, urban heat stress and heat island mapping studies in complete cities [13]. These studies are usually ordered by governmental institutions with wide purposes, and they are not commonly affordable by citizens for their particular needs.

With the appearance of low-cost unmanned aerial vehicles (UAVs), different research groups have started to use this technology to program photogrammetry flights and generate 3D point clouds and digital terrain models (DTM) from the digital imagery acquired of medium size areas [14–15]. Regarding the use of thermographic cameras, some studies have approached the use of UAVs for the geometric – thermographic inspection of façades, acquiring data difficult to reach from a terrestrial point of view, but missing important information of the roof [16]. What is more, multispectral cameras have been used for agricultural purposes, [17–18], such as monitoring the application of herbicide in turf grass and detection and classification of greenhouses.

This paper proposes the extension of the thermographic studies performed in individual building façades, to the inspection of the building roofs, at a larger scale: medium-size areas such as neighbourhoods, villages or districts using a low-cost aerial platform, UAV-type. Due to this enlargement in the scale, land uses other than buildings can be analysed, consequently widening the application of the proposed methodology from energy efficiency in buildings to fields such as land and water management, agriculture monitoring, detection of greenhouses, forest exploitation, etc.

In the proposed study, data acquired is used to generate a thermographic mosaic and texture a digital terrain model, allowing for the identification of different land uses, such as buildings, forest and grass area, their spatial contextuali-

*e-mail: susiminas@uvigo.es

zation and characterization. The structure of the paper is as follows: Section 2 explains the proposed methodology, including both data acquisition and data processing for the generation of thermographic mosaics covering larger areas than images individually and its inclusion in a digital terrain model (DTM); Section 3 presents the procedure use for the classification of the thermographic DTM's as a function of the different land uses; Section 4 discusses the quality of the results obtained with the proposed procedure regarding methods currently under use. Finally, Section 5 includes the conclusions reached after the performance of the study.

2. Methodology

2.1. Data acquisition

The platform chosen for the aerial inspection has been provided by HiSystems GmbH [19]. It is an eight-propeller copter, referred to as Okto XL, chosen due to its high payload, its high robustness to motor failure, its easiness of manoeuver in difficult outdoor scenes, and its low-cost [20].

The copter consists on a frame of aluminium squared tubes and carbon fibre base plates, powered by eight brushless motors with the capability of driving both left and right.

However, although the payload is among the greatest for these kind of vehicles, its value of 2 kilograms is still a restrictive factor when choosing a thermographic sensor to mount on (Fig. 1). Because of its compromise between lightweight and thermal resolution, a thermographic camera Gobi384 was selected for this work. It has a 384×288 uncooled microbolometer array able to acquire with a frame rate of up to 50 fps. Thanks to its high acquisition speed, the flight speed of the copter is not limited and acquisition of thermographic images of all the area flight is assured. The camera is equipped with a thermographic lens with 10 mm focal length, providing a field of view of 51°×40°.

The study area is located in the municipality of Vigo, province of Pontevedra, in the Northwest of Spain (Fig. 2). It comprises an area of about 26.000 m^2 at the south of the city, and is centred on the WGS84 geographic coordinates of 42°10'11"N and 8°41'23"W.

The area selected for the flight is a mountainous zone with dispersed buildings, in such a way that different land uses are acquired (rural zones and buildings), allowing for the analysis of the spectral responses in the thermal infrared band of the different terrains.

Fig. 1. UAV equipped with thermographic camera.

The flight was planned taking into account the field of view of the camera and the overlap desired between consecutive strips, considering as a strip each long flying line that forms the complete path followed by the UAV. Given these factors, a flight height of 50 meters, and 4 strips was the configuration needed. The flight planning can be seen in Fig. 3.

The weather conditions for the flight must be in agreement with the requirements of both the copter and the thermography: that is, on a no-rainy day, with light wind and in a moment when there is not direct sun on the surface, so that there is no heterogeneous heating affecting the surface and consequently distorting the measurements.

For the area covered, a flight of only 5 minutes is needed at an average speed of 5m/s, in which more than 14000 images are acquired, each covering an approximate area of 48×48 m^2 according to the angular field of view of the camera lens and the flight height. What is more, the pixel size under these conditions is 15 cm^2, which allows for the identification of individual trees and bushes, as well as most of the building elements present in the roof: chimneys, antennas and air conditioning systems, among others.

Fig. 2. Location of the area selected for the study.

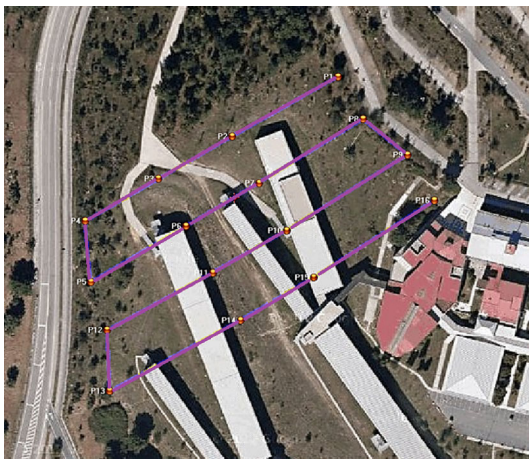

Fig. 3. Flight planning for thermographic image acquisition. Red dots identify the control points established to avoid the deviation of the copter within one strip.

2.2. Thermographic mosaicking

Thermographic images are formed by only one matrix with temperature values; regarding image format it would be as if the value of each pixel was a temperature value. Taking the smallest and the largest temperature values appearing in the image, the matrix can be scaled, so that all values range between 0 and 1. Then, a 3-channel colour palette can be applied, so that thermographic images are converted to images in the RGB colour space with colours related to temperature values. Once this conversion is performed, images can be subjected to the mosaicking process.

The first step of the process is the generation of a thermographic mosaic of the area, with which the digital terrain model can be textured. The mosaic is generated using proprietary software made in Matlab® and an orthophotograph as a support, from RGB-thermographic images chosen among all those acquired. The selection of thermographic images for the mosaic is performed in such a way that the images cover all the area under study with a minimum overlap of 50% between adjacent thermographies. For the selected thermographies distortion added by the sensor is corrected prior further processing, thanks to the geometric calibration of the camera-lens system, performed as in Ref. 21. The calibration parameters of the thermographic camera used in the inspection are shown in Table 1.

For the correction of radial distortion, the unbalanced lens model is considered; distortion is calculated with Eqs. (1)–(3), where x, y are the image coordinates of each pixel, and r is the radial position of the pixel, calculated as the sum $x^2 + y^2$.

$$\text{Radial distortion: } dr = r + K_1*r^2 + K_2*r^4 + K_3*r^6; \quad (1)$$

$$\text{Tangential distortion in the X-axis: } dp_x = P_x*(r^2+2x^2) + 2*P_y*x*y; \quad (2)$$

$$\text{Tangential distortion on the Y-axis: } dp_y = P_y*(r^2+2y^2) + 2*Px*x*y. \quad (3)$$

Table 1. Geometric calibration parameters of the thermographic camera Gobi 384 used for data acquisition.

Pixel size (mm/pix)		0.0156
Format size (mm)		5.9997 (W) × 4.5000 (H)
Principal point (mm)	X_p	2.8807
	Y_p	2.2891
Radial distortion	K_1	–0.1142
	K_2	2.924e–3
	K_3	0
Tangential distortion	P_x	–1.813e–4
	P_y	–9.998e–5

Once radial distortion is corrected from the selected images, image registration is performed for each thermography by marking control points between thermographies and the orthophotograph of the selected area; this process is refined by the calculation of the correlation value between each pair of points, followed by the search of points that maximize this value within an area of 7×7 pixels for each thermography. This value is chosen for being the smallest area size that maximizes the precision of the result of correlation [22]. After registration, perspective effects appearing in the original thermography are corrected and the registered images have the same resolution as the reference orthophotograph. The registration process is shown in Fig. 4.

Once all thermographies are registered, they are put together into the same mosaic image, so that all the flown area is covered. Pixel values in overlapping regions between adjoining images are specifically calculated in order to avoid edge seam. Thus, a linear transition method (LTM) is applied [23]. This LTM method calculates the value of each pixel as a weighed mean of the pixel in each image, using as weigh the distance of the pixel in the thermographic mosaic to the image centre of each image composing the mosaic, Eq. (4).

$$M_i = (X_{max}–X_i)/(X_{max}–X_{min})*A_i + [1– (X_{max}–X_i)/(X_{max}–X_{min})]*B_i. \quad (4)$$

If images are adjacent, in the same row X_{max} and X_{min} stand for the maximum and minimum value of X in the overlapping area. Where A_i denotes the value of pixel *i* in image *A*, and B_i the value of pixel *i* in image *B*. The position of pixel *i* in image A is denoted as X_i, and the homogenized pixel value is M_i.

An example of the process of thermographic mosaic generation is shown in Fig. 5.

2.3. Thermographic digital terrain modelling

The thermographic mosaic generated is ready to be imported in a spatial mapping software such as ArcGis©. The mosaic is directly imported and geo-referenced before being used to texture a conventional DTM. Furthermore, the ther-

Fig. 4. Image registration process (left); registered image (right).

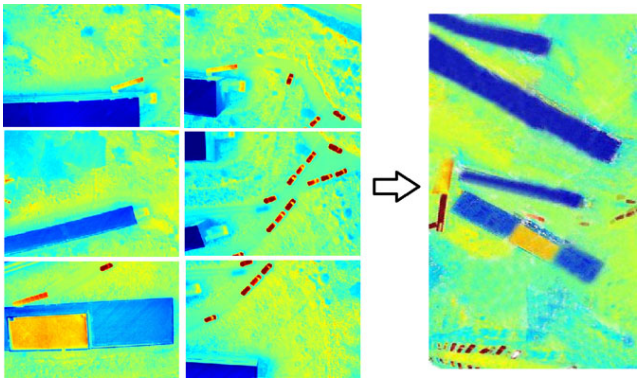

Fig. 5. Thermographic mosaic generation.

mographic mosaic can be fused with an orthophotograph of the area in order to obtain both visual and thermal information in a spatial context (Fig. 6). Image fusion can be performed with different approaches; in this case, the thermographic image is converted to IHS colour space (intensity, hue, saturation), and the intensity channel is substituted by the orthophotograph in grayscale. The fused image GHS (gray level, hue, saturation) is then reconverted to the original RGB colour space. With this procedure, the resulting image presents the colour information of the thermographic image, with the geometrical resolution of the orthophotograph.

3. Land-use classification

The generated thermographic digital terrain model allows for the detection of four buildings in the flight area (in blue), together with a parking area, and rural area with different types of vegetation: warmer areas, in yellow, correspond to low-height vegetation such as grass, whereas colder areas, in green and light blue, correspond to taller vegetation, from bushes to trees.

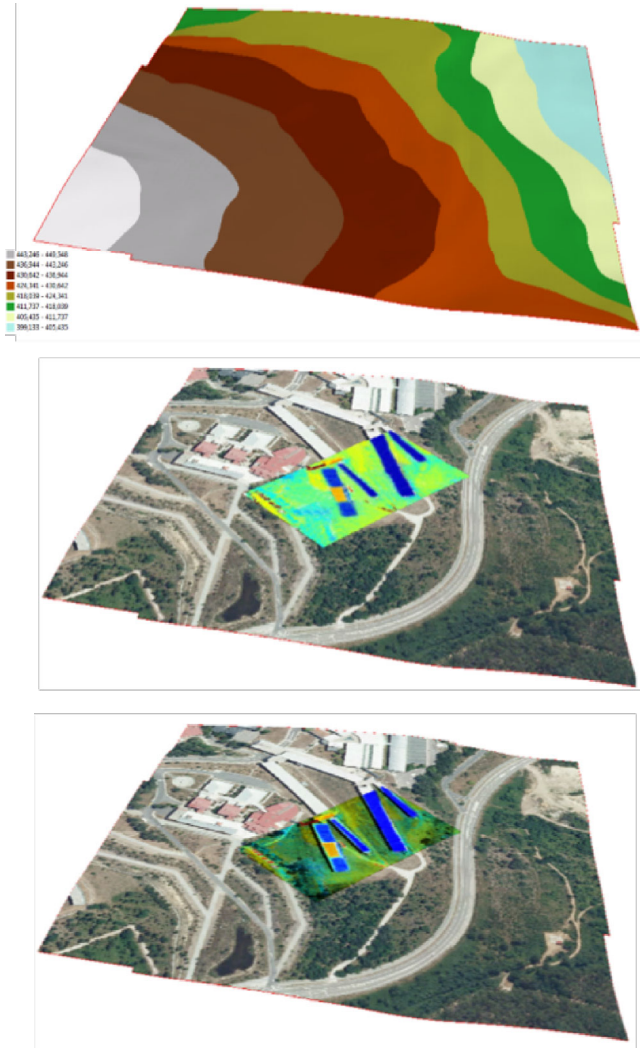

Fig. 6. Thermographic DTM generation carried out in ArcGIS©. From top to bottom: conventional DTM, DTM textured with the thermographic mosaic, texture completed with the orthophotograph, and DTM textured with an image resulting from the fusion of a thermography with an orthophotograph.

Given that the terrain presents different temperature according to its use, pixel classification is performed in the thermographic DTM, so that the area affected by each use is automatically calculated. Pixel segmentation is based on the conversion of the image, in RGB colour space, to XYZ colour space [24]. Other colour spaces such as YCbCr can be used for the conversion, but in this work the XYZ colour space is chosen due to its device-independent nature, allowing the performance of identical segmentation analysis in every device.

In this colour space, each pixel X is a measure of the stimulus of red, Y measures luminosity, and Z indicates the stimulus of blue. Consequently, if we convert the image to the XYZ colour space and focus on the X, Z values, pixels can be classified merely according to their chromaticity. In the area under study, three different groups have been selected: buildings, low-height vegetation, and tall vegetation (bushes and trees) (Fig. 7). After this, pixels that have been classified in a group where they do not belong are removed from each cluster using a threshold value for colour; this step is especially important in the low-height vegetation cluster (Fig. 7, Cluster 2), since it includes pixels corresponding to concrete paths for vehicles.

Knowing the value of the pixel size of the DTM (25 cm/pixel) and the number of pixels of each use provides the area dedicated: metal roofs (Fig. 7, Cluster 1) occupy 4650 m^2, for 100 m^2 of non-metal roofs. These surface values, together with the surface temperatures measured in the thermographic images and the ambient conditions, allow for the identification of the material of the roof, so that the quantity of heat lost to the atmosphere (by convection and radiation heat transfer methods) through the building's roof can be computed [Eq. (5)].

$$Q = h_{roof}*A*(T_{roof}–T_{ext}) + 4*\varepsilon*\sigma*A*T^4_{roof}\,. \qquad (5)$$

Being Q the quantity of heat lost to the atmosphere, h_{roof} the thermal convective coefficient of the outer part of the roof (units W/m^2K), A the area of the roof, T_{roof} the temperature of the outer surface of the roof measured in the thermographic images, and T_{ext} the ambient temperature. For the computation of the radioactive heat, ε is the emissivity value of the outer surface of the roof, and σ is the Boltzmann constant, equal to $5.67e^{-8}$ W/m^2K^4.

Regarding environment, and following the same approach as with buildings, a value of 8050 m^2 and 13240 m^2 is obtained for the areas destined to tall and low vegetation, respectively.

4. Results and discussion

The validity of the proposed methodology is checked by comparing the surface values obtained per land use with reality. Consequently, official maps from the National Cartographic Institute [25] are used as a reference (Fig. 8), and the surfaces corresponding to the 3 different land uses are measured in the official orthophotograph of the area. Results are shown in Table 2, where an error lower than 5% can be seen for the three cases.

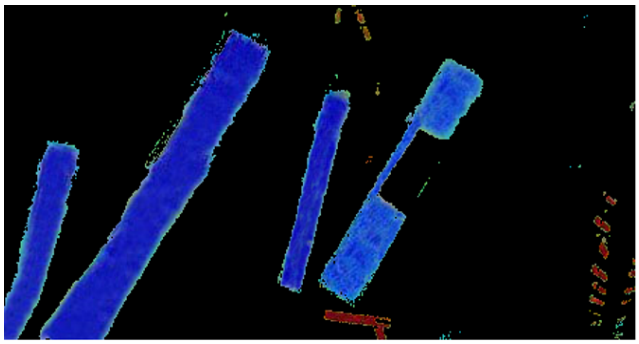

Cluster 1

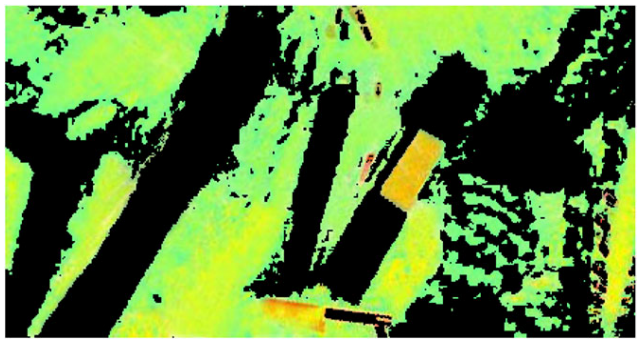

Cluster 2

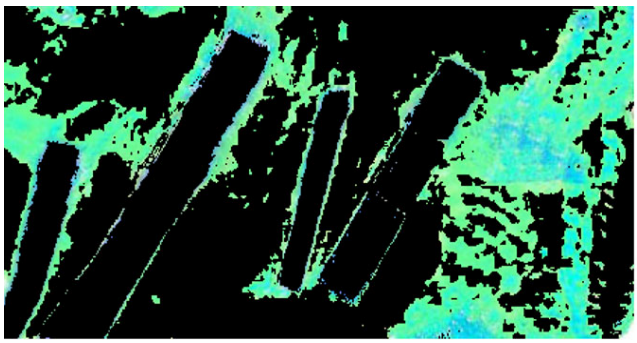

Cluster 3

Fig. 7. Different clusters obtained after the conversion of the thermographic DTM to XYZ colour space.

Table 2. Accuracy results of the proposed methodology.

Land use	Real value (m^2)	Value from methodology (m^2)	% deviation
Building roof	4.932	4.750	3.69
Low vegetation	12.644	13.240	4.71
Tall vegetation	8.391	8.050	4.06

5. Conclusions

This paper presents a methodology for the generation of a thermographic terrain model using a low-cost aerial platform, copter-type.

The result of the registration and mosaicking of the thermographies acquired from the air, followed by the use of the mosaic for texturing the digital terrain model, is

Fig. 8. Detail of the orthophoto containing the area under study. PNOA given by © Instituto Geográfico Nacional de España.

a thermographic DTM in which several analysis can be performed: the different spectral responses in the thermal infrared band of each type of terrain allows for the identification and segmentation of the different land uses existing in the area. What is more, the knowledge of the pixel size of the resulting thermographic DTM provides geometric information of the total area, and consequently, of the area corresponding to each land use.

Surface calculation is the base step for further studies such as heat losses of buildings, individually or in a medium scale (small towns, districts and neighbourhoods). In the agricultural field, the knowledge of the area covered per use increases the accuracy in crop calculation, as well as land and water management, and irrigation planning. On the other hand, the combination of the surface value with the topography given by the DTM, can be used for the quantification of forest masses and evaluation of possible future uses of the vegetation area.

The limitations of the proposed methodology are mainly technological: the area covered is limited by the flight autonomy of the aerial vehicle used, which is 15–30 minutes for the vehicles currently in the market, also depending on the mounted payload. Regarding data processing, the step of image registration increases significantly the working time due to the fact of being manual, which also makes the accuracy of the whole process dependent on the operator skills. Although the first drawback can only be solved by time and technological progress, the second drawback regarding manual processing can be dealt with future work, focusing on the automation of the feature extraction and the identification of corresponding entities between images.

Regarding the capabilities of the proposed methodology, future work will focus on the exploitation of the thermographic DTM through the extraction of parameters of interest of each object present: coordinates of buildings, evaluation of heat islands, identification of tree species, evaluation of land state (water irrigation, terrain fertility), detection of buried objects, etc.

Acknowledgements

Authors would like to give thanks to the Consellería de Economía e Industria (Xunta de Galicia), Ministerio de Economía y Competitividad and CDTI (Gobierno de España) for the financial support given through human resources grants (FPDI–2013–17516, FPU AP2010–2969), and projects (IPT2012–1092–120000, ITC–20133033, ENE2013–48015–C3–1–R). All the programs are co-financed by the Fondo Europeo para el Desarrollo Regional (FEDER).

References

1. T. Taylor, J. Counsell, and S. Gill, "Energy efficiency is more than skin deep: Improving construction quality control in new-build housing using thermography", *Energ. Buildings* **66**, 222–231 (2013).
2. F. Asdrubali, G. Baldinelli, and F. Bianchi, "A quantitative methodology to evaluate thermal bridges in buildings", *Appl. Energ*. **97**, 365–373 2012.
3. E. Grinzato, N. Ludwig, G. Cadelano, M. Bertucci, M. Gargano, and P. Bison, "Infrared thermography for moisture detection: a laboratory study and in-situ test", *Mater. Eval*. **69**, 97–104 (2011).
4. S. Chudzik, "Thermal diffusivity measurement of insulating material using infrared thermography", *Opto-Electron. Rev*. **20**, 40–46 2012.
5. P. Bison and E. Grinzato, "IR thermography applied to the assessment of thermal conductivity of building materials", in *32th Thermosense*, Orlando, 2010.
6. P. Fokaides and S. Kalogirou, "Application of infrared thermography for the determination of the overall heat transfer coefficient (U-value) in building envelopes", *Appl. Energ*. **88**, 4358–4365 (2011).
7. A. Bortolin, G. Cadelano, G. Ferrarini, and P. Bison, "Thermal performance measurement of the building envelope by infrared thermography", *AITA Conference*, Torino, 2013.
8. S. Lagüela, L. Díaz-Vilariño, J. Martínez, and J. Armesto, "Automatic thermographic and RGB texture of as-built BIM for energy rehabilitation purposes", *Automat. Constr*. 31, 230–240 (2013).
9. Y. Ham and M. Golparvar-Fard, "EPAR: Energy Performance Augmented Reality models for identification of building energy performance deviations between actual measurements and simulation results", *Energ. Buildings* 63, 15–28 (2013).
10. M. Scaioni, E. Rosina, L. Barazzetti, M. Previtali, and V. Redaelli, "High-resolution texturing of building façades with thermal images", in *34th Thermosense*, Baltimore, 2012.
11. L. Hoegner and U. Stilla, "Automatic generation of façade textures from terrestrial thermal infrared image sequences", *QIRT*, Bordeaux, 2014.
12. F. Agüera, F. Aguilar, and M. Aguilar, "Using texture analysis to improve per-pixel classification of very high resolution

images for mapping plastic greenhouses", *ISPRS J. Photogrammetry and Remote Sensing* **63**, 635–646 (2008).
13. J.E. Nichol and P. Hang To, "Temporal characteristics of thermal satellite images for urban heat stress and heat island mapping", *ISPRS J. Photogrammetry and Remote Sensing* **74**, 153–162 (2012).
14. N. Haala, M. Cramer, F. Weimer, and M. Trittler, "Performance test on UAV based photogrammetric data collection", *IAPRS* **38** (1/C22) 7–12 (2011).
15. F. Neitzel and J. Klonowski, "Mobile 3D mapping with a low-cost UAV system", *IAPRS* **38** (1/C22), 39–44 (2011).
16. M. Previtali, L. Barazzetti, and R. Brumana, "Thermographic analysis from UAV platforms for energy efficiency retrofit applications", *J. Mobile Multimedia* **9**, 66–82 (2013).
17. H. Xiang and L. Tian, "Development of a low-cost agricultural remote sensing system based on an autonomous unmanned aerial vehicle (UAV)", *Biosyst. Eng.* **108**, 174–190 (2011).
18. M. Aguilar, F. Bianconi, F. Aguilar, and I. Fernández, "Object-based greenhouse classification from GeoEye-1 and WorldView-2 stereo imagery", *Remote Sensing* **6**, 3554–3582 (2014).
19. Wiki Mikrokopter: mikrokopter.de. Last access: 04/04/2013.
20. D. Roca, S. Lagüela, L. Díaz-Vilariño, J. Armesto, and P. Arias, "Low-cost aerial unit for outdoor inspection of building façades", *Automat. Constr.* **36**, 128–135 (2013).
21. S. Lagüela, H. González-Jorge, J. Armesto, and J. Herráez, "High performance grid for the metric calibration of thermographic cameras", *Measurement Science and Technology* **23**, 9 (2012).
22. E. Coll, J. Martínez, and J. Herráez, "The determination matrix size for videogrammetry correlation", *Conf. Advances in Signal Processing, Robotics and Communications*, pp. 56–59, Malta, 2001.
23. S. Lagüela, J. Armesto, P. Arias, and J. Herráez, "Automation of thermographic 3D modelling through image fusion and image matching techniques", *Automat. Constr.* **27**, 24–31 (2012).
24. CIE, *Colorimetry*, CIE Publication 15.2, 2nd Ed, pp. 19–20, 56–58, Vienna, 1986.
25. Instituto Geográfico Nacional. Centro Nacional de Información Geográfica: www.ign.es. Last access: 09/07/2014.